AN ANALYSIS OF ITERATIVE ALGORITHMS FOR IMAGE RECONSTRUCTION FROM SATELLITE EARTH REMOTE SENSING DATA

Matthew H Willis
Brigham Young University, MERS Laboratory
459 CB, Provo, UT 84602
801-378-4884, FAX: 801-378-6586, willism@et.byu.edu

Abstract

This paper discusses algorithms for creating enhanced-resolution images from satellite earth remote sensing data. The well-known ART and MART algorithms are discussed, as well as a new class of algorithms—*column-normalized* algorithms. The SART algorithm is studied as an example of a column-normalized algorithm and is compared structurally to the SIR algorithm to help explain SIR's success at remote sensing image reconstruction. Several reconstruction algorithms are then compared using both simulated and real satellite radiometer data sets.

Introduction

With humankind's recent interest in global climatology and the impact that we have made on our environment, there is a pressing need for fast, accurate measurements of key global parameters such as ocean wind speed, ocean height, and land and ice characteristics. Some of the land and ice characteristics that are of interest include snow-cover classification, plant and soil moisture content, vegetation classification, and polar ice-extent mapping.

Microwave satellite instruments, such as radiometers and scatterometers, play an important role in helping determine these key global parameters. The advantage of microwave instruments is that they can take measurements of the earth's surface day or night and are not affected by cloud cover. Another advantage of these instruments is their rapid repeat coverage, with the recent QuickScat scatterometer being able to cover almost the entire earth in one day.

The tradeoff for the fast coverage of radiometers and scatterometers is their low spatial resolution. Radiometer and scatterometer measurements over the ocean have been used successfully for generating numerical weather-prediction model data and determining ocean wind speed, but low resolution has limited their use in land and ice studies. However, by applying resolution enhancement algorithms to the data, images with sufficient resolution for land and ice studies can be obtained.

Problem Description

Figure 1 illustrates the remote sensing imaging problem. First, the observed image is discretized into

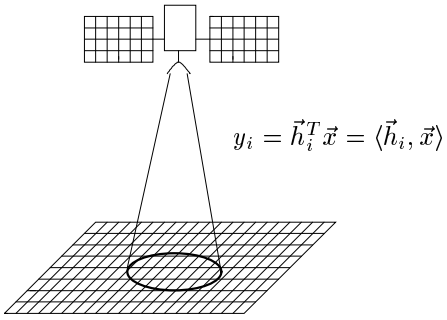

Figure 1: Geometry of image reconstruction in remote sensing

pixels. Each measurement is the received microwave signal from the area on the ground multiplied by the antenna aperture function at each pixel. In the case of a radiometer, this observation is the weighted average of the radiometric brightness temperature of the pixels in the aperture multiplied by the antenna response at that pixel. For a scatterometer, a weighted average over the illuminated region is observed as the microwave backscatter. The value of the i'th measurement, y_i, then, is $y_i = \langle \vec{x}, \vec{h}_i \rangle$ where $\langle \cdot, \cdot \rangle$ denotes the standard inner product, $\vec{x}$ is the row-scanned image, and $\vec{h}_i$ contains information about the value and location of the antenna footprint, such that h_{ij} represents the contribution of the j'th pixel to the i'th measurement.

The measurements are stacked up to yield

$$\vec{y} = \mathcal{H}\vec{x} \tag{1}$$

where $y : \mathbb{R}^m$ is the measurement vector, and $\mathcal{H} : \mathbb{R}^{m \times n}$ is the point spread matrix, or transfer matrix. The remote sensing imaging problem is to find an estimate $\hat{x}$ given $\vec{y}$ and $\mathcal{H}$. In general, direct inversion of $\mathcal{H}$ to solve for $\hat{x}$ is not possible because the matrix $\mathcal{H}$ is often too large to fit in its entirety in computer memory, and also because $\mathcal{H}$ may be underdetermined and have no unique inverse. While the least-squares pseudo-inverse exists for inverting an underdetermined matrix, the least-squares solution may not be the most desirable solution. These issues suggest using an iterative algorithm to invert $\mathcal{H}$.

For the rest of this report I will drop the vector symbol notation, with the understanding that variables without subscripts are understood to be vectors with the exception of h_i, which is the i'th row of $\mathcal{H}$.

Algebraic Reconstruction Techniques

Reconstructing an image from a set of measurements, as is done in the remote sensing imaging problem, is called *image reconstruction projections*. Algorithms for reconstructing images from projections have been used in the medical imaging community since the early 1970s for reconstructing Computerized Tomography (CT) and electron microscopy images [1],[2]. One class of algorithms used in medical imaging is algebraic reconstruction techniques, which iteratively invert the matrix $\mathcal{H}$ to find $\hat{x}$. Two common reconstruction methods in this class of algorithms are the Algebraic Reconstruction Technique (ART) and the Multiplicative ART (MART) algorithms.

The ART algorithm has been proved to converge to a least-squares solution [3], satisfying the constrained minimization problem

$$\min_x \| x \|_2^2 \quad \text{such that} \quad y = \mathcal{H}x. \tag{2}$$

The algorithm update is as follows:
Initialization: $x^\circ = 0$
Iterative step:

$$x_j^{k+1} = x_j^k + \frac{y_i - \langle h_i, x^k \rangle}{\| h_i \|} h_{ij} \tag{3}$$

where x_j^k is the jth element of the vector x at the kth iteration, h_i is the ith row of $\mathcal{H}$, and h_{ij} is the (i,j)th element of $\mathcal{H}$. Only one row of $\mathcal{H}$—h_i—is needed for each iteration, such that only one row of $\mathcal{H}$ needs to be stored in the computer's memory at a time, making it practical for reconstructing systems where $\mathcal{H}$ is large.

MART, another popular algorithm, is a Maximum Entropy (ME) algorithm, satisfying the constrained optimization

$$\min_x \sum_x x \ln x \quad \text{such that} \quad \mathcal{H}x = y, \tag{4}$$

where $\sum_x x \ln x$ is the negative of the information theoretic entropy. The algorithm update is as follows:
Initialization: $x^\circ = \exp(-1)$
Iterative step:

$$x_j^{k+1} = x_j^k \left(\frac{y_i}{\langle h_i, x^k \rangle} \right)^{\lambda_1 h_{ij}}. \tag{5}$$

Column-normalized Algorithms

For the past several years the Brigham Young University Microwave Earth Remote Sensing (BYU MERS) Lab has been using image reconstruction algorithms to create enhanced-resolution images of the earth's surface. ART and MART were found to suffer from sampling artifacts and noise amplification, limiting their use for remote sensing image reconstruction. In response, the MERS lab developed the Scatterometer Image Reconstruction Technique (SIR) for image reconstruction. The SIR update is shown in the following lines:
Initialization: $x^\circ =$ arbitrary.
Iterative step

$$x_j^{k+1} = \frac{\sum_{i=1}^{M} u_{ij}^k h_{ij}}{\sum_{i=1}^{M} h_{ij}}, \tag{6}$$

or

$$x_j^{k+1} = \frac{\mathcal{H}_j^T u_{ij}}{\mathcal{H}_j^T \mathbf{1}} \tag{7}$$

in matrix form, where $\mathcal{H}_j$ is the jth column of $\mathcal{H}$ and $\mathbf{1}$ is a vector of ones. The nonlinear update term u_{ij} is given by

$$u_{ij}^k = \begin{cases} \left[\frac{1}{2 f_i^k} \left(1 - \frac{1}{d_i^k} \right) + \frac{1}{x_j^k d_i^k} \right]^{-1} & d_i^k \geq 1 \\ \left[\frac{1}{2} f_i^k (1 - d_i^k) + x_j^k d_i^k \right] & d_i^k < 1. \end{cases} \tag{8}$$

where d_i^k is the fidelity term

$$d_i^k = \left(\frac{y_i}{\langle h_i, x^k \rangle} \right)$$

and f_i^k is the forward projection $\langle h_i, x^k \rangle$.

SIR performs very well for image reconstruction, suppressing sampling artifacts and noise. However,

at the time of SIR's development the reasons for its success were not well understood.

Another algorithm that has shown promise for remote sensing image reconstruction is the Simultaneous ART (SART) algorithm, who's update is given in matrix form in the following lines:
Initialization: $x^\circ = 0$.
Iterative step

$$x_j^{k+1} = x_j^k + \frac{\mathcal{H}_j^T d^k}{\mathcal{H}_j^T \mathbf{1}}, \tag{9}$$

where

$$d_i^k = y_i - \langle h_i, x^k \rangle. \tag{10}$$

SART was proposed by Andersen and Kak as a method for CT image reconstruction with effective artifact suppression characteristics [4],[5]. In my thesis, I prove that SART converges to a *weighted least-squares* solution, satisfying the constrained optimization problem

$$\min_x \sum_j \frac{x_j^2 H_j^T \mathbf{1}}{2} \quad \text{such that} \quad y - \mathcal{H}x. \tag{11}$$

This weighting of the j'th pixel by the sum of the elements in the jth column of $\mathcal{H}$, which contains the sampling information (number of times sampled and the weighting at each sample) for that pixel, appears to reduce sampling artifacts and noise in the reconstructed image. The weighting in Eq. (11) is a result of the normalization of the SART update in Eq. (9) by $\mathcal{H}_j^T \mathbf{1} = \sum_j h_{ij}$, the sum of the columns of $\mathcal{H}$.

Since the SIR update has the same normalization, we suspect that its success at artifact and noise suppression is also due the normalization. We have named this class of algorithms, which normalize the update by the columns of $\mathcal{H}$, *column-normalized* algorithms. Column-normalized algorithms appears to be an appropriate class of algorithms for remote sensing image reconstruction.

Reconstruction Results

In this section, six algorithms are compared when reconstructing simulated and real data—ART, ART with modified median filter (ARTF), SART, SART with modified median filter (SARTF), SIR, and SIR with modified median filter (SIRF). The modified median filter, which selects the median intensity when there is a wide range of pixel values in the window and computes an average when there is a narrow range of values, was developed in conjunction with SIR and was found to control the noise level in the reconstructed images.

The synthetic truth image used for simulation is shown in Figure 2. For realistic simulations, a sampling grid matched to the SSM/I satellite radiometer sampling grid over an Amazon region is used (see Figure 4). The measurements are taken from Julian day 190 to 194 in 1999, during which time there were 2604 measurements taken of the earth's surface. Figure 3 shows the instrument sampling over the region of interest for the specified day range. The noisy measurements were created by adding $\sigma = .0036$ i.i.d., white, Gaussian noise the the noise-free measurements, resulting in a signal-to-noise ratio (SNR) of 45.0 dB.

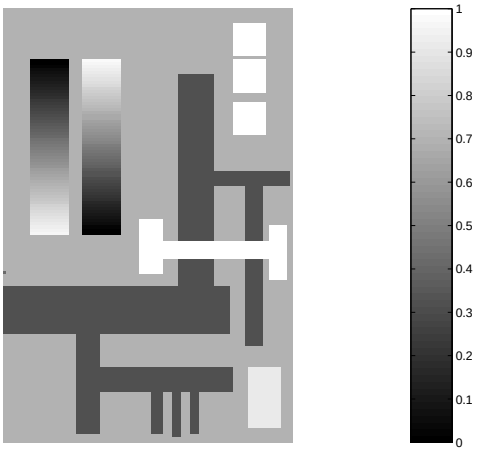

Figure 2: The original synthetic "truth image" used for simulations

Figures 5, 6, and 7 show the results for the noise free simulation, the noisy simulation, and the real data respectively. All of the algorithms reconstruct the simulated data well, but ART has the worst artifact and noise suppression. The SIR and SART reconstructions are very similar, which similarity may be a result of the column normalization in their iterative update.

The results of the reconstructions from real data are more interesting. While SIR and SART do comparable jobs of reconstructing the image, the ART reconstruction is quite poor. ART may not reconstruct the image well for several possible reasons:

- There may be discrepancies between the actual antenna footprint and the footprint model used for reconstruction, causing inconsistencies in the system.

- Noise in the system corrupts the image.

- Because the measurements are taken over a range of days, the ground image is not stationary, which will result in more inconsistencies.

The above scenarios would worsen the performance of all of the algorithms, but as Figures 5 and 6 indicate, ART inherently suffers more from artifacts and noise than do the column-normalized algorithms.

Conclusion

This paper discussed different algorithms which can be used for remote sensing image reconstruction to create enhanced resolution images of the earth's surface. A class of algorithms, called column-normalized algorithms, was discussed, and reconstruction results from both simulated and real data indicate that column-normalized algorithms may be more appropriate than ART or MART for remote sensing image reconstruction.

References

[1] R. Gordon, R. Bender, and G.T. Herman, "Algebraic reconstruction technique (ART) for three-dimensional electron microscopy and x-ray photography", *J. Theoret. Biol*, vol. 29, pp. 471–481, 1970.

[2] P. Gilbert, "Iterative methods for the three-dimensional reconstruction of an object from projections", *J. Theoret. Biol*, vol. 36, pp. 105–117, 1972.

[3] G.T. Herman and A. Lent, "ART, mathematics and applications", *J. Theo. Biol.*, vol. 42, pp. 24–32, 1973.

[4] A.H. Andersen and A.C. Kak, "Simultaneous algebraic reconstruction technique (SART): A superior implementation of the ART algorithm", *Ultrasonic Imaging*, 1984.

[5] A.H. Andersen, "Algebraic reconstruction in CT from limited views", *IEEE Trans. on Med. Img.*, vol. 8, no. 1, pp. 50–55, March 1989.

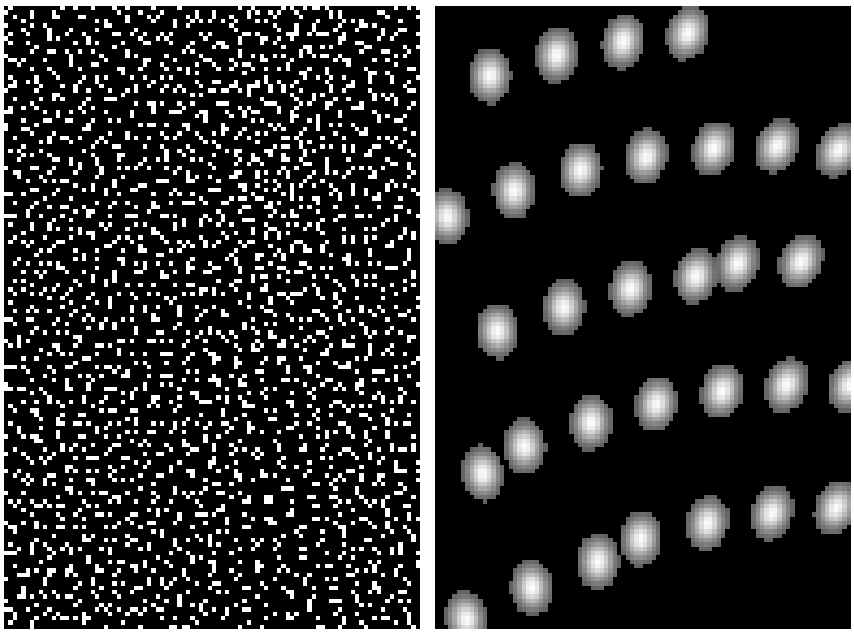

Figure 3: SSM/I sampling geometry—The dots in the left figure indicate the center of each footprint. The right figure shows a view of some representative footprints (both figures are on the same scale).

Figure 4: The area in the black rectangle represents the region in the Amazon basin from which the measurement geometries are taken (the area is magnified at the bottom right hand corner of the image).

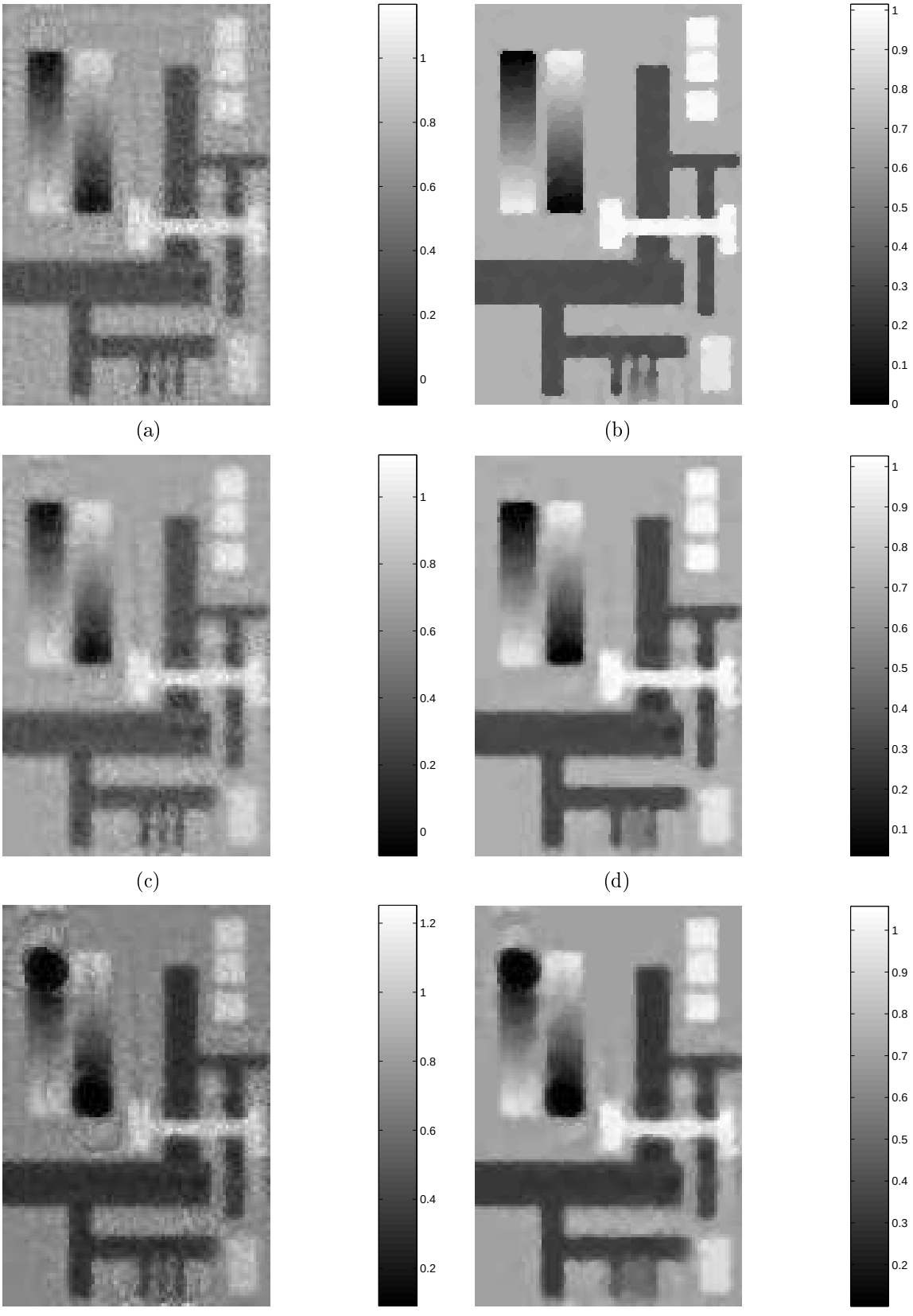

Figure 5: Noiseless reconstructions for SSM/I sampling geometry using (a) ART (b) ART with filter (ARTF) (c) SART (d) SART with filter (SARTF) (e) SIR (f) SIR with filter (SIRF)

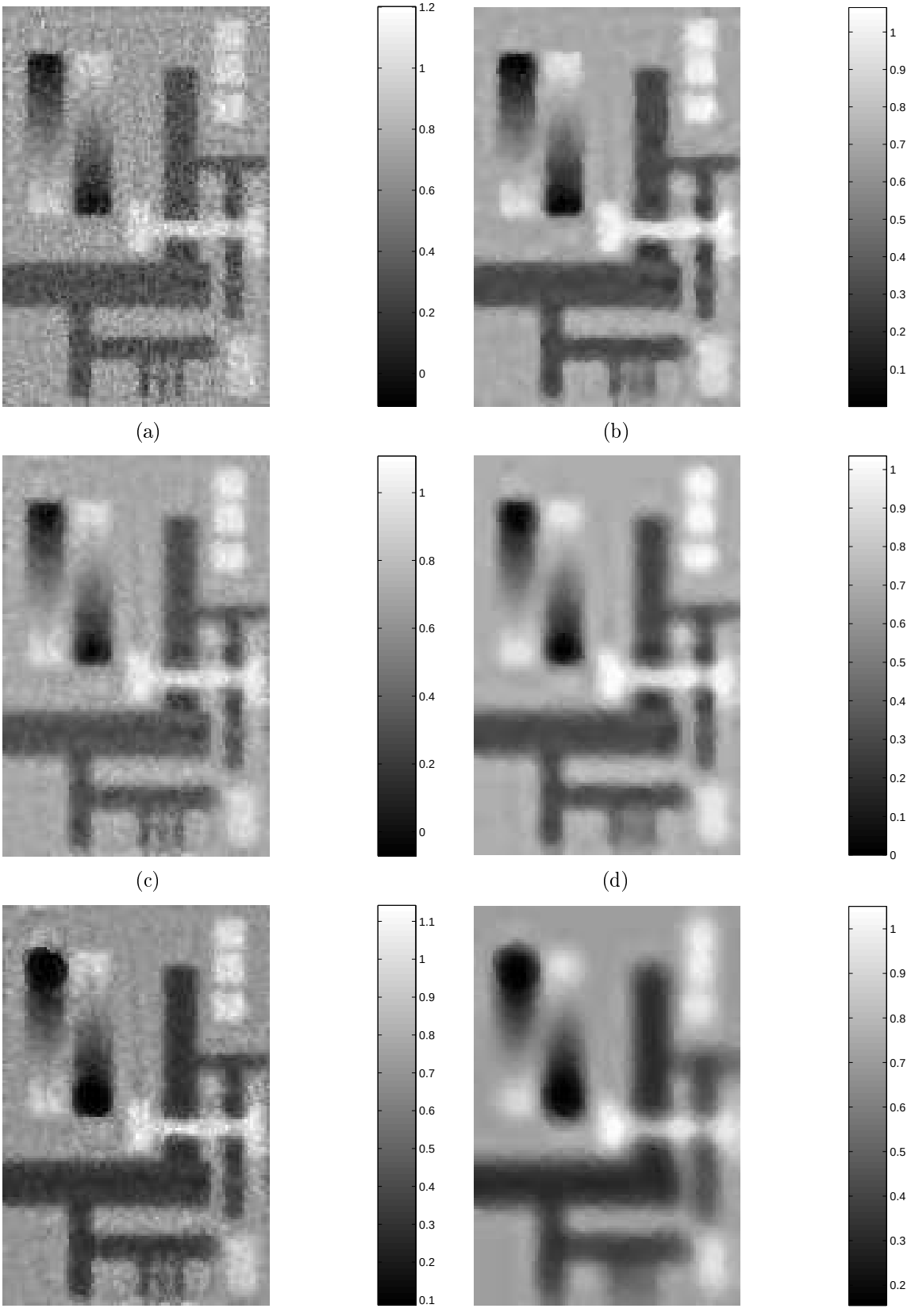

Figure 6: 45.0 dB SNR SSM/I geometry reconstruction using (a) ART—20 iterations (b) ART with filter (ARTF)—12 iterations (c) SART—1058 iterations (d) SART with filter (SARTF)—50 iterations (e) SIR—694 iterations (f) SIR with filter (SIRF)—27 iterations

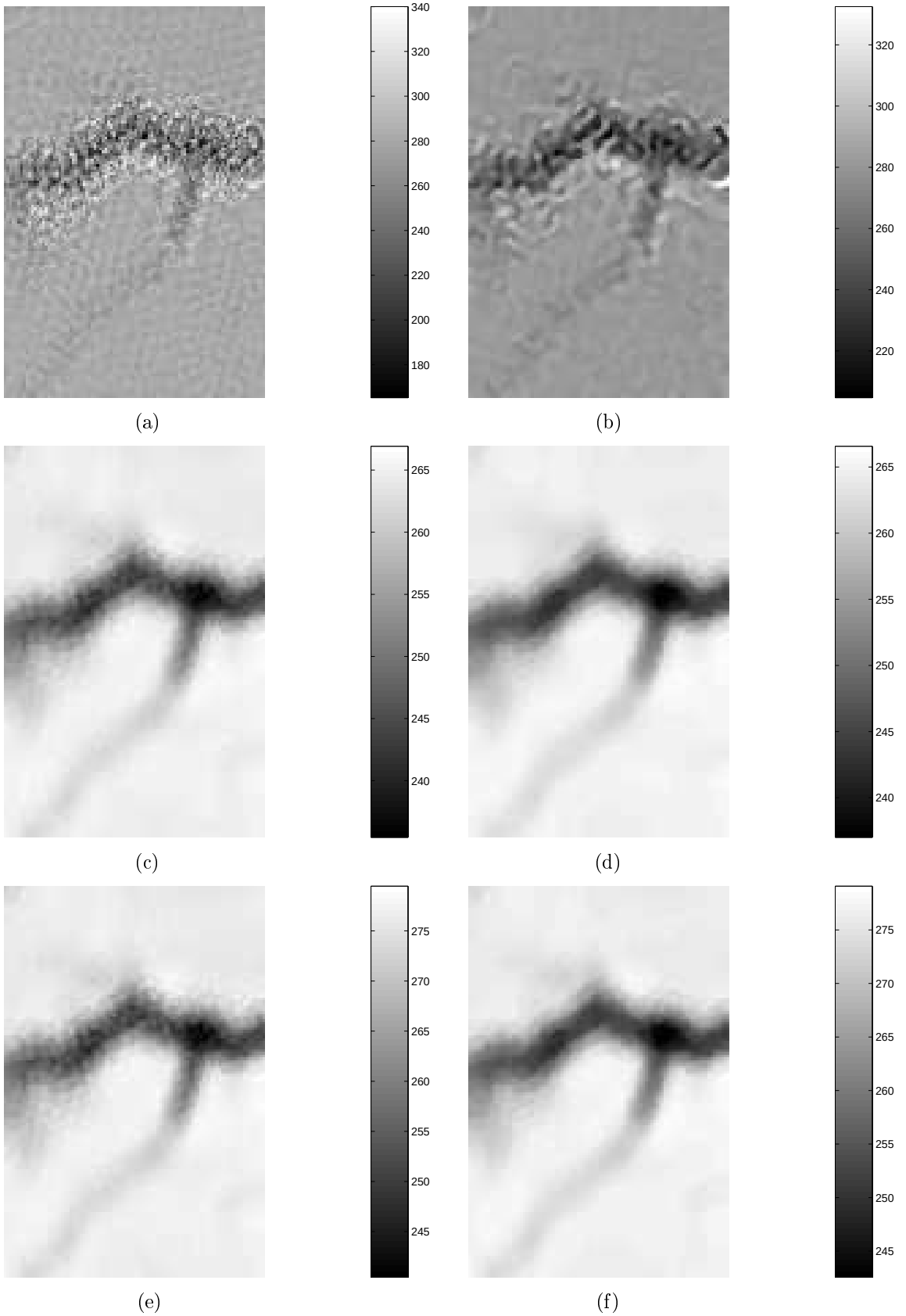

Figure 7: Reconstruction of real SSM/I data using (a) ART—5 iterations (b) ARTF—15 iterations (c) SART—30 iterations (d) SARTF—30 iterations (e) SIR—10 iterations (f) SIRF—10 iterations